Rotationally resolved studies of S_0 and the exciton coupled S_1/S_2 origin regions of diphenylmethane and the d_{12} isotopologue

Jaime A. Stearns,[1] Nathan R. Pillsbury,[2] Kevin O. Douglass,[3] Christian W. Müller,[2] Timothy S. Zwier,[2] and David F. Plusquellic[3,a]

[1]*Laboratoire Chimie Physique Moléculaire, École Polytechnique Fédérale de Lausanne, CH-1015 Lausanne, Switzerland*
[2]*Department of Chemistry, Purdue University, West Lafayette, Indiana 47907, USA*
[3]*Biophysics Group, Optical Technology Division, National Institute of Standards and Technology, Gaithersburg, Maryland 20899-8441, USA*

Rotationally resolved microwave and ultraviolet spectra of jet-cooled diphenylmethane (DPM) and DPM-d_{12} have been obtained in S_0, S_1, and S_2 electronic states using Fourier-transform microwave and UV laser/molecular beam spectrometers. The S_0 and S_1 states of both isotopologues have been well fit to asymmetric rotor Hamiltonians that include only Watson distortion parameters. The transition dipole moment (TDM) orientations of DPM and DPM-d_{12} are perpendicular to the C_2 symmetry axes with 66(2)%:34(2)% a:c hybrid-type character, establishing the lower exciton S_1 origin as a completely delocalized, antisymmetric combination of the zero-order locally excited states of the toluene-like chromophores. In contrast, the rotational structures of the S_2 origin bands at S_1+123 cm^{-1} and S_1+116 cm^{-1}, respectively, display b-type Q-branch transitions and lack the central a-type Q-branch features that characterize the S_1 origins, indicating TDM orientations parallel to the $C_2(b)$ symmetry axes as anticipated for the upper exciton levels. However, rotational fits were not possible in line with expectations from previous work [N. R. Pillsbury, J. A. Stearns, C. W. Müller, T. S. Zwier, and D. F. Plusquellic, J. Chem. Phys. **129**, 114301 (2008)] where the S_2 origins were found to be largely perturbed through vibronic interactions with the S_1 symmetric, antisymmetric torsional, and butterfly levels in close proximity. Predictions from a dipole-dipole coupling model and *ab initio* theories are shown to be in fair agreement with the observed TDM orientations and exciton splitting. The need to include out-of-ring-plane dipole coupling terms indicates that in-plane models are not sufficient to fully account for the excitonic interactions in this bichromophore. © 2008 American Institute of Physics. [DOI: 10.1063/1.3028543]

I. INTRODUCTION

Investigations of exciton coupling between two (or more) interacting chromophores have been of long-standing interest in both gas and condensed phase environments.[1–21] Diphenylmethane (DPM) has served as a prototypical molecule for such studies.[1,2] The (π-π^*) nature of the lowest electronic transitions together with the three lowest frequency inter-ring modes associated with the torsional τ and bending α degrees of freedom (see Fig. 1) makes for intriguing consequences regarding the dependence of the excitonic interactions on these coordinates. For example, excitonic interactions in the perpendicular ring configurations found in the benzene dimer[3] or spirobifluorene[4] are expected to be vastly different from those in a face-to-face arrangement of the D_{2h} naphthalene dimer in the crystal[5,6] because of the sensitive nature of molecular orbital overlap factors and the geometric dependence of the interaction terms. Such fundamental studies of electronic coupling between chromophores are needed to validate and refine models used for interpretation of the photophysics of excimer formation of gas-phase torsional isomers,[7] electroluminescence and solar energy conversion in conjugated organic semiconductors,[8,9] fluorescence resonance energy transfer data from single molecule measurements of protein folding,[10] hysteresis (I-V) properties of molecular electronic devices,[11] and other areas of solid state physics such as exciton-polariton propagation in crystals.[12]

Previous calculations[13] on DPM found that it possesses two enantiomeric minima of C_2 symmetry with the rings at dihedral angles of approximately 60° with respect to the C(Ph)–CH$_2$–C(Ph) plane. Figure 1 illustrates one of the structurally chiral isomers of DPM. The corresponding two-dimensional (2D) ground state torsional potential energy surface is shown in Fig. 2, calculated on an 18×18 (10°) grid at the MP2/6-311++G** level of theory. The minima are separated by a C_{2v} transition state which is picturesquely described as a "gable" structure. There also exists a low energy transition state of C_s symmetry in which the rings are perpendicular to one another. Both transition states were calculated to be less than 250 cm^{-1} above the minima at the MP2/6-311++G** level of theory.[14]

The issue of exciton coupling in bichromophores has a long experimental and theoretical history.[1,2,5,14–21] Electronic coupling is usually discussed in terms of either excitonic interactions, meaning the coupling and splitting of degener-

a)Electronic mail: david.plusquellic@nist.gov.

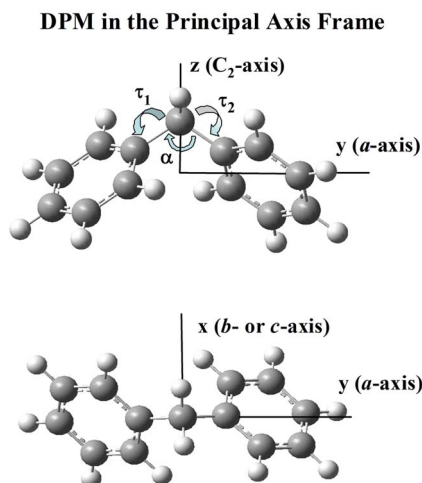**DPM in the Principal Axis Frame**

FIG. 1. (Color online) Structure of DPM in the principal axis frame. The three soft degrees of freedom associated with the lowest frequency modes are shown and include the two torsional coordinates τ_1 and τ_2 defined as the dihedral angle between the planes formed by Ph–CH$_2$–Ph and the three ring carbon atoms nearest to the methylene group and the coordinate α defined as the Ph–CH$_2$–Ph bend (butterfly).

ate electronic states due to identical chromophores in a molecule, or electronic energy transfer between chromophores which are largely unperturbed by each other. However, the underlying coupling in each case is the same.[5] In either case, the discussion of the electronic states begins by designating the two chromophores A and B. The zero-order locally excited electronic states are then written $|A^*B\rangle$ and $|AB^*\rangle$ where electronic excitation is indicated by an asterisk. For the case of DPM, in which the chromophores are identical, the inclusion of a matrix element coupling the two localized excitation states results in the exciton states,
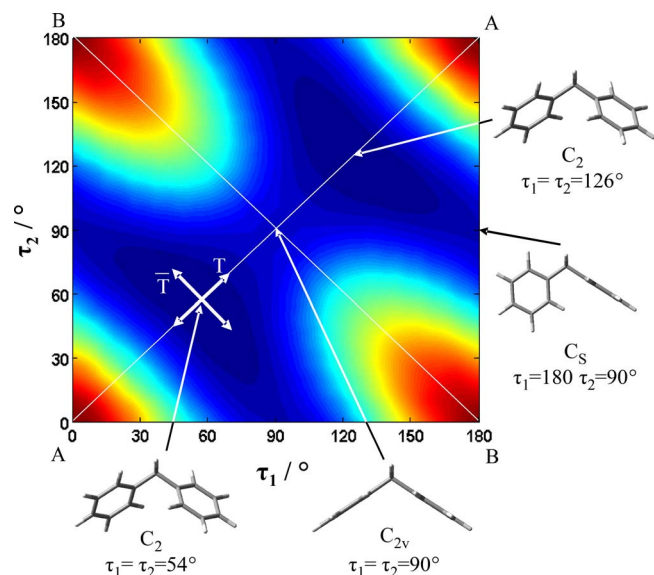

FIG. 2. (Color online) Ground state torsional potential energy surface for DPM calculated at the MP2/6-311++G** level of theory. The axes represent the torsion angles of the phenyl rings, τ_1 and τ_2. The phenyl torsional normal mode displacement directions T (symmetric) and $\bar{T}$ (antisymmetric) are shown by double-headed arrows. The structures associated with the two enantiomeric C_2 minima, the C_{2v} gable transition state, and the perpendicular C_s transition state are all shown.

$$\psi_{\pm} = \frac{1}{\sqrt{2}}(|A^*B\rangle \pm |AB^*\rangle). \tag{1}$$

The resulting energy splitting between ψ_+ and ψ_- is determined by the magnitude of the matrix element connecting the two localized excited states,

$$H_{12} = \langle A^*B|H|AB^*\rangle. \tag{2}$$

The contributions to H_{12} depend on the separation and relative orientation of the chromophores' transition dipole moments (TDMs). At short intermonomer distances, orbital overlap becomes important and penetration and exchange terms must be included.[5] Most analyses, however, include only the long-range, or Coulombic, interaction. Specifically, the electronic excitation on one chromophore creates a polarization of the electron density of the other, which is described by a TDM on either phenyl ring. The TDM on the two chromophores can be approximated by two interacting point dipoles, giving the usual expression[5]

$$V_{dd} = \frac{\mu_A \mu_B}{4\pi\varepsilon_0 R^3}(2\cos\theta_A\cos\theta_B + \sin\theta_A\sin\theta_B\cos\phi), \tag{3}$$

where μ is the magnitude of the TDM of the localized chromophore, R is the intermonomer separation, θ is the angle the localized TDM makes with the intermonomer axis, and φ is the dihedral angle between the localized TDMs. The overall TDM for the bichromophore in the exciton states is given by the sum and difference of the localized TDMs. Recently, Eq. (3) has been used successfully to describe coupling in spirobifluorene[4] and the 2-pyridone dimer.[20,21]

Application of Eq. (3) to DPM is particularly interesting because the orientations and relative interactions of the zero-order TDMs are dependent on the relative orientation of the phenyl rings. As Fig. 2 shows, the symmetric gable structure ($\tau_1=\tau_2=90°$) would have excited electronic states in which the electronic excitation is delocalized over the two rings, while the C_s symmetry perpendicular structure ($\tau_1=180°$, $\tau_2=90°$) would have electronic excitations that are localized on either the top or stem of the "tee."

McClure[1,2] cast Eq. (3) in terms of a torsion angle $\tau \equiv \tau_1 = \tau_2$, assuming a value for α (see Fig. 1) and localized toluene-like TDM orientations perpendicular to the C–CH$_2$ axes of the rings. The exciton splitting and overall TDM for each of the two exciton states were then calculated as a function of τ and the results were used to interpret the absorption spectrum of a DPM crystal at low temperatures. The spectrum showed a weak absorption 145 cm^{-1} above the S_1 origin that was attributed to the upper member of the exciton doublet. A torsion angle τ of 60° was determined (note that $\tau=30°$ in the convention used in McClure's[2] work). If DPM is assumed to be a strongly coupled, delocalized system with C_2 symmetry, one exciton state will have a TDM parallel to the C_2 axis, and thus that state will have A symmetry. The other exciton state will have a TDM in the plane perpendicular to the C_2 axis, and that state will have B symmetry. McClure[2] deduced from Eq. (3) and a localized toluene-like TDM orientation that the A state must lie below the B state in

crystalline DPM. However, the state order is actually the opposite in the gas phase as a result of significant rotation of the localized TDM away from that of toluene as we will show below.

In a previous paper (hereafter referred to as Paper I),[14] resonant two-photon ionization (R2PI) and single vibronic level fluorescence (SVLF) spectroscopy of DPM and DPM-d_{12} were used to identify the S_2 origins and assign all three of the lowest frequency modes in the S_0, S_1, and S_2 electronic states. The SVLF spectra of the S_2 origin and S_2 vibronic bands were found to contain emission from S_1 vibronic levels having S_2 state symmetry at relative energies within 10 cm^{-1} of the S_2 level. Analysis of these data permitted the assignment of the coupled modes and determination of the approximate magnitudes of the coupling matrix elements and the mixed state character of the S_2 states resulting from internal mixing with the S_1 levels.

In this work, we have used rotationally resolved spectroscopies to study the S_0, S_1, and S_2 origin bands of DPM and DPM-d_{12} in the unperturbed environment of the molecular beam. The rotationally resolved data have provided additional insight into the structure and electronic symmetries of the exciton coupled state pairs. Specifically, we seek a full analysis of the microwave (MW) and UV spectra to aid in determining the S_0 geometries and changes that occur in the S_1 and S_2 states and to interpret the observed TDM orientations in terms of the dipole-dipole coupling model given by Eq. (3). While these goals were only partially realized for the S_2 spectra because of the perturbations arising from the S_1/S_2 state mixing, qualitative features of these spectra are shown to be entirely consistent with the prior SVLF work.[14] Interpretations of the observed TDM orientations and exciton splitting have been aided by extensive calculations of the ground and excited state torsional surfaces.

II. EXPERIMENTAL METHODS

Rotationally resolved fluorescence excitation spectra of DPM and its isotopologue, DPM-d_{12}, were measured using an UV laser/molecular beam spectrometer described in detail elsewhere.[22] Briefly, an Ar$^+$-pumped (488 nm line) cw ring dye laser using Coumarin 521 (Ref. 23) generated ≈500 mW of narrow band light (≈1 MHz) near 534 nm. Approximately 3 mW of the UV light at 267 nm was generated in an external resonant cavity containing a β-barium borate crystal. DPM was heated to 393 K (120 °C) in a three chamber quartz source. Typically, the vapor was mixed with 21–29 kPa, 160–220 Torr of Ar gas and expanded into a source chamber through a 125 μm nozzle (the S_1 origin of DPM was obtained using 29 kPa of a He/Ne mixture). The molecular beam was skimmed and crossed at right angles with a slightly focused UV beam 18 cm downstream of the source. Laser induced fluorescence at the beam crossing was collected with 20% efficiency using two spherical mirrors[24] and detected using a photomultiplier and computer interfaced photon counter. The Doppler limited resolution of the spectrometer using Ar carrier gas is 18(1) MHz at 330 nm (Ref. 25) and is therefore expected to be 21(1) MHz at 267 nm. Relative frequency calibration was performed using a HeNe

stabilized reference cavity[26] and absolute frequencies were obtained using a wavemeter accurate to ±0.02 cm^{-1}. DPM was available commercially and used at the stated purity of 99%. DPM-d_{12} was synthesized in the laboratory according to the procedure outlined in the supplemental material of Ref. 14.

The pure rotational spectrum of DPM-h_{12} was recorded in a mini-Fourier-transform microwave (MW) spectrometer[27] operating between 11 and 18 GHz. Because of the small dipole moment predicted for DPM (<0.05 D), the MW excitation circuit was modified to include a preamplifier and a 1 W power amplifier followed by a p-i-n diode MW switch. Optimal excitation was achieved using ~25 mW of MW power and a 2 μs polarizing pulse. Samples were loaded into a heated reservoir nozzle and heated to 433 K (160 °C) for DPM.

Electronic structure calculations were carried out using GAUSSIAN03.[28] The 2D ground state surface shown in Fig. 2 was constructed on a grid of stationary points obtained at the MP2/6-311++G** level of theory. Excited state single point calculations were carried out using time-dependent density functional theory (TD-DFT)/6-311++G** at the optimized ground state geometries. The GAMESS computational package was used to carry out complete active space self-consistent field (CASSCF)/6-31G* calculations.[29] Eight electrons were distributed among eight orbitals, those π and π^* orbitals corresponding to linear combinations of the toluene-like highest occupied molecular orbitals and lowest unoccupied molecular orbitals on each ring.

III. RESULTS AND ANALYSIS

A. The ground state and S_1 origin bands of DPM and DPM-d_{12}

The rotationally resolved spectra of the $S_1 \leftarrow S_0$ band origins of DPM and DPM-d_{12} at 267.9 nm (37 322.1 cm^{-1}) and 266.6 nm (37 506.8 cm^{-1}) are shown in Figs. 3 and 4, respectively. These spectra were fit using a combination of techniques. The initial fits were performed using a distributed parallel version of the genetic algorithm (GA) program.[30] Estimates of the ground state rotational constants were obtained from *ab initio* theory (*vide infra*). Prominent features in these spectra permitted estimates of key excited state parameters. For example, the initial GA runs included only a-type selection rules because of the strong central a-type Q branches observed and reasonable ranges were placed on the parameter differences in S_1 from the Q-branch shading and $(B+C)$ level spacing. Once the rotational constants were sufficiently well determined by the GA, the hybrid band character was then fit.

The residuals from the best fit simulated spectra are shown below the experimental data in Figs. 3 and 4 and a summary of the rotational constants and other parameters is given in Table I. Expanded portions of these spectra adjacent to the central Q-branch regions are shown in the lower panels of Figs. 3 and 4. The residuals demonstrate that the origin bands of DPM and DPM-d_{12} are both a:c hybrid bands with 66(2)%:34(2)% character, respectively. Residuals also shown for simulations having a:b:c hybrid band intensities of
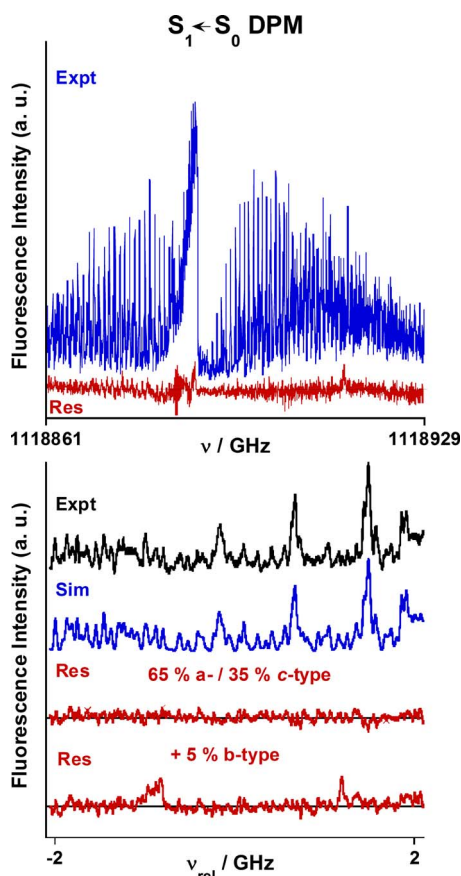
FIG. 3. (Color online) Rotationally resolved spectrum of the $S_1 \leftarrow S_0$ origin band of DPM-h_{12}. The full spectrum is shown in the top panel with residuals (Res). The residuals with and without 5% *b*-type character over an expanded portion blue of the central *a*-type *Q* branch in the lower panel illustrates the complete absence of *b*-type character.
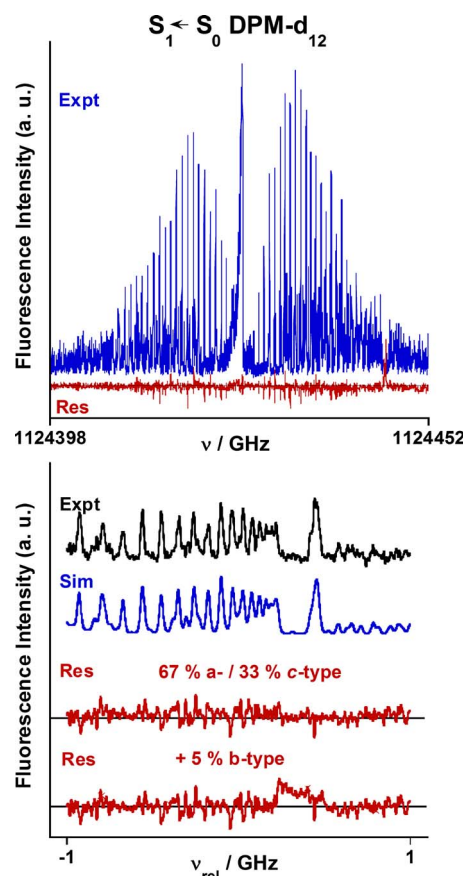
FIG. 4. (Color online) Rotationally resolved spectrum of the $S_1 \leftarrow S_0$ origin band in DPM-d_{12}. The full spectrum is shown in the top panel with residuals (Res). The residuals with and without 5% *b*-type character over an expanded portion blue of the central *a*-type *Q* branch in the lower panel illustrates the complete absence of *b*-type character.

$\approx 63\%:5\%:32\%$ (i.e., with 5% *b*-type character added) aid in establishing an upper limit of 2% *b*-type character for both S_1 origins.

Predictions based on these ground state parameters were used to locate and measure selected lines in the MW spectrum of DPM. Using the linear least-squares fitting procedure implemented in the JB95 program,[31] 35 pure rotational transitions were required in representation I^r to determine all five of the first-order Watson distortion parameters reported in Table I. Furthermore, slightly improved fits were realized in the symmetric reduction for this nearly accidental prolate symmetric top.

Because of the size of DPM, most rotational transitions in the UV spectra were unresolved, making isolated line assignments rare. Therefore, frequencies were assigned in combination with refinements in the other (nonlinear) parameters affecting intensities in the following way. Using more restricted ranges ($\pm 0.5\%$) for the rotational constants in the GA program, the TDM components, axis reorientation angle, temperature parameters,[32] and Lorentzian or Gaussian width were simultaneously varied. For these runs, all S_0 parameters of DPM in Table I were held fixed and the S_0 distortion parameters of DPM were used for fits of DPM-d_{12}. Simulated spectra were generated from the average parameters over ten GA runs and experimental assignments were made based on the line profiles. The final S_1 parameters that in-

clude distortion terms are given in Table I for each isotopologue with uncertainties in the final digit corresponding to type A, $k=1$ or 1σ. The uncertainties of the intensity parameters were confirmed in nonlinear least-squares fits of these spectra.[31] It is noted that despite the similar magnitudes of the ground state *B* and *C* rotational constants, the *b* and *c* axes do not interchange upon electronic excitation.

The possibility of line splitting from tunneling through the low transition state barriers shown in Fig. 2 warrants some mention of the linewidths observed in the MW and UV spectra. In contrast to the ≈ 1 MHz splitting observed for the MW spectrum of the isoelectronic bichromophore, diphenyl ether,[33] tunneling splittings in DPM are less than 3 kHz although some line broadening is noted. In S_1, the fluorescence lifetime has been estimated near 40 ns from fluorescence decay measurements using a pulsed nanosecond neodymium doped yttrium aluminum garnet laser in a jet,[14] which corresponds to a Lorentzian width ($\Delta \nu_L$) of ≈ 4 MHz. For DPM-d_{12} in an Ar gas expansion, $\Delta \nu_L$ was fitted to 7(2) MHz and in reasonable agreement with the lifetime data given the large Doppler contribution, $\Delta \nu_G \approx 21(2)$ MHz, and limited 1 MHz digital resolution of the data. For DPM, the instrumental Doppler width of a He/Ne carrier gas is unknown and therefore, $\Delta \nu_G$ for DPM was fit to 32(5) MHz. In either case,

TABLE I. Rotational constants and distortion parameters from least-squares fits of the ground state and S_1 $\leftarrow S_0$ origin spectra of DPM-h_{12} and DPM-d_{12}. The S_0 parameters of DPM-h_{12} were determined from fits of the MW spectrum. Other parameters were determined from the UV spectra using a combination of techniques that made use of GA and nonlinear least-squares fitting routines (see text for details).

	DPM-h_{12}		DPM-d_{12}	
	S_0	S_1	S_0	S_1
$A''/\Delta A$ (MHz)	2036.5283(9)	−5.381(2)	1682.07(3)	−3.750(7)
$B''/\Delta B$ (MHz)	423.1649(2)	2.382(5)	382.31(4)	2.632(5)
$C''/\Delta C$ (MHz)	421.4613(2)	−6.103(4)	381.74(3)	−5.584(5)
$\Delta I''/\Delta \Delta I$ (u Å^2) [a]	−243.3295(9)	23.64(1)	−298.47(1)	28.02(2)
$\Delta_J/\Delta\Delta_J$ (MHz)	6.35(4)×10⁻⁵	−7.4(9)×10⁻⁶	⋯ [b]	−1.2(4)×10⁻⁵
$\Delta_{JK}/\Delta\Delta_{JK}$ (MHz)	7.6(4)×10⁻⁵	−3.03(3)×10⁻⁴	⋯ [b]	−2.4(1)×10⁻⁴
$\Delta_K/\Delta\Delta_K$ (MHz)	3.75(3)×10⁻³	−9.85(2)×10⁻⁴	⋯ [b]	−5.7(2)×10⁻⁴
$\delta_1/\Delta\delta_1$ (MHz)[c]	1.336(8)×10⁻⁵	−8.6(6)×10⁻⁶	⋯ [b]	⋯ [b]
$\delta_2/\Delta\delta_2$ (MHz)[c]	−1.68(5)×10⁻⁶	6.8(6)×10⁻⁷	⋯ [b]	⋯ [b]
Origin (cm⁻¹)	⋯	37322.10(2)	37 506.80(2)/ + 184.70(2)	
Band type (%)	100 b	65(2) a: 35(2) c	67(2) a: 33(2) c	
$\Delta v_G/\Delta v_L$ (MHz)[d]	⋯	32(1)/4	21.3/7(2)	
$T_1:T_2$ (K)	2	8.9(2)/32(1)	2.7(2)/8.8(5)	
wt[e]		0.41(2)	0.34(3)	
$\theta_{a/c\ \text{reorient}}$ (deg)[f]	⋯	−0.674(6)	−0.859(11)	
Assigned	35	203	298	
σ (MHz)	0.0022	0.37	0.47	

[a]Inertial defect $\Delta I = 505,379(1/C - 1/A - 1/B)$, where $A = \hbar^2/2I_a$ and I_a is the moment of inertia about the a axis, etc.
[b]Values fixed at the ground state values determined from fits of the MW spectrum of DPM.
[c]Symmetric reduction used in both states. For S_0, σ increased to 2.6 kHz in the asymmetric reduction.
[d]Voigt lineshape includes the Doppler (Gaussian), Δv_G, and Lorentzian (lifetime), Δv_L, components (full width at half maximum). For DPM-h_{12}, Δv_L is fixed at the value determined from lifetime measurements. For DPM-d_{12}, Δv_G is fixed at the measured value with frequency correction in an Ar carrier gas expansion.
[e]Two temperature model from Ref. 32: $\exp(-\Delta E/kT_1) + wt \exp(-\Delta E/kT_2)$.
[f]Angle represents the upper state frame rotation about the b axis relative to the lower state with negative angles corresponding to a counterclockwise rotation.

line broadening was minimal, establishing an upper limit of ≈2–3 MHz for the tunneling splitting through the C_{2v} transition state in S_1.

The absence of b-type character in the spectra of DPM-h_{12} and DPM-d_{12} indicates retention of C_2 symmetry in both electronic states (*vide infra*). As a result of this symmetry, nuclear spin statistical weights are potentially important factors that could impact the transition intensities. Since no tunneling splittings were observed, the permutation-inversion group is G_4, which is isomorphic with C_{2v}. The nuclear spin statistical weights of the K_aK_c ee(oo):eo(oe) (e =even, o=odd) levels are calculated to be 65:63 in DPM-h_{12} and 730:728 ee(oo):eo(oe) for DPM-d_{12}. At the signal-to-noise ratios of our measurements, these intensity differences are too small to be observed.

B. The S_2 origin bands of DPM and DPM-d_{12}

Rotationally resolved S_2 origin band spectra of DPM and DPM-d_{12} are located at 267.0 nm (S_1+123 cm⁻¹) and 265.8 nm (S_1+116 cm⁻¹) [14] and shown in Figs. 5 and 6, respectively. The overall integrated intensities of these bands are much weaker than the corresponding S_1 origins and therefore, experiments were repeated on several occasions to enhance the signal-to-noise ratios. The frequency control system of the laser enabled scans obtained under the same expansion conditions but over a period of several months to

be coaveraged. Furthermore, to aid in the analysis, spectra of DPM were obtained at two different rotational temperatures. The lower trace in Fig. 5 was obtained under similar conditions used for the S_1 origin of DPM-d_{12} while the upper trace was obtained under warmer expansion conditions using a lower expansion gas pressure of 21 kPa (160 Torr). Clear differences are evident in the relative intensities of sharp features and in the overall appearance of these two spectra where the width is seen to increase from ≈3 to >4 cm⁻¹ under the warmer expansion conditions. The overall shape of the DPM-d_{12} spectrum shown in Fig. 6 is much different, with intensity pileups separated by ≈1 cm⁻¹. However, because of the limited amount of sample, this spectrum was obtained at a much lower signal-to-noise ratio (≈5:1) compared to the DPM spectrum (≈30:1) and therefore, a detailed analysis of this band is not discussed further.

Given the overall spectral complexity of these bands, it is first necessary to arrive at some expectation about the appropriate rovibronic selection rules. From the SVLF and hot band results discussed in Paper I,[14] the two origin bands in Figs. 5 and 6 have been assigned to the upper exciton S_2 states. If the S_1 and S_2 electronic states have C_2 point group symmetry, are strongly coupled, and therefore are delocalized over both toluene-like subgroups, the resulting exciton states, ψ_+ and ψ_-, from Eq. (1) will have A and B symme-
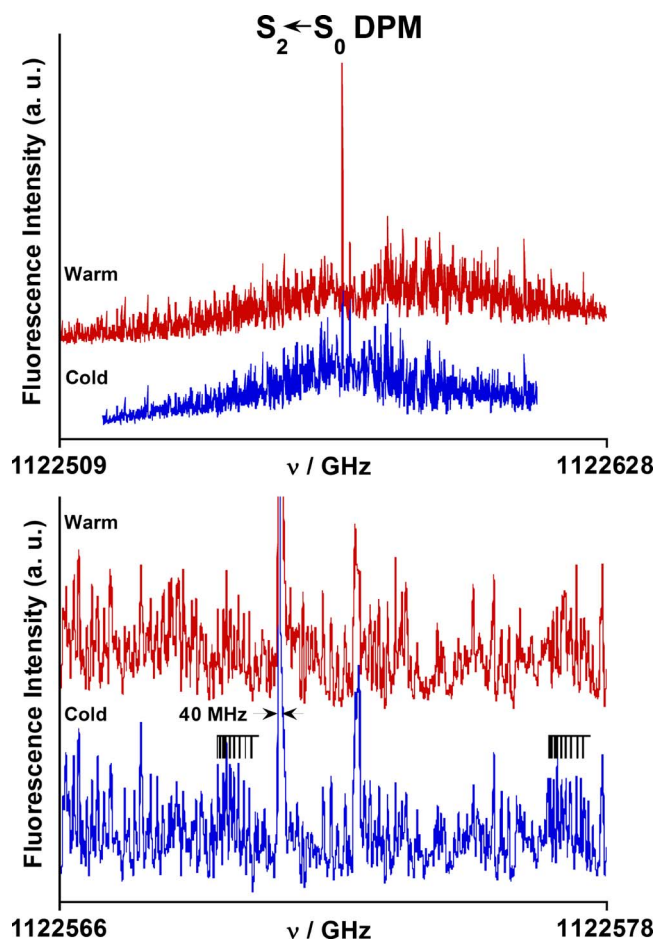
FIG. 5. (Color online) Rotationally resolved spectrum of the $S_2 \leftarrow S_0$ origin band in DPM (upper panel) and an expanded region near the center of this band (lower panel). The top spectrum in each panel was obtained under warmer expansion conditions and compared with the lower spectrum obtained under similar conditions used for the S_1 origin of DPM-d_{12}. The two sets of tie lines in the lower panel designate progressions that closely resemble b-type Q-branch series in the quantum number J.

tries, respectively. Since the S_1 states of DPM and DPM-d_{12} have been fitted to a:c hybrid bands having TDM orientations perpendicular to the C_2 symmetry axes (*vide infra*), the S_1 states must be ψ_-, i.e., the antisymmetric combination in Eq. (1). Therefore, the S_2 origin bands are expected to be the ψ_+ exciton states having A symmetry and TDM orientations parallel to the $C_2(b)$ symmetry axes. In these cases, fits that include only b-type rotational selection rules should apply.
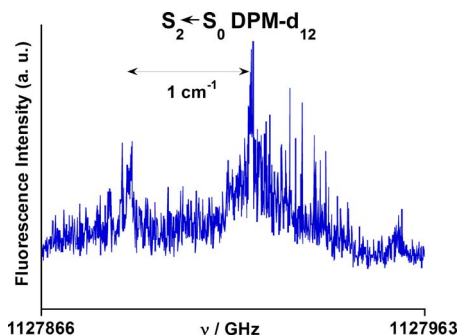

FIG. 6. (Color online) Rotationally resolved spectrum of the $S_2 \leftarrow S_0$ origin band in DPM-d_{12}. The spectrum was obtained under similar conditions used for the S_1 origin of DPM-d_{12}.

Consistent with these arguments, there is a clear absence in the S_2 origin bands of the central Q-branch features and the P- and R-branch ($K_a=0$, $K_c=J$) progressions that characterize the a-type TDM components of both S_1 origins. An expanded 12 GHz section that illustrates the central features of the cold spectrum of DPM is shown in the lower panel of Fig. 5. Although significant spectral congestion exists throughout this region, the widths of many of the rotational lines are near the 21 MHz Doppler limit of the instrument for an Ar gas expansion. The dominant sharp feature (shown off scale in the lower panel) is only ≈ 40 MHz in width and much too narrow to be an a-type Q branch. It is likely the result of a b-type J series band head. For comparison, the Q-branch widths of the S_1 states are both >500 MHz.

Other patterns in the expanded region are more readily identified as belonging to a b-type rotational band. For example, the two progressions indicated with tie lines in the lower panel are easily modeled as a b-type Q-branch ($\Delta J=0$, $\Delta K_a=+1/-1$, $\Delta K_c=-1/+1$) series in J. Similar progressions appear to be present in the S_2 spectrum of DPM-d_{12}. Such well separated Q-branch series rarely if ever occur in a-type bands ($\Delta K_a=0$, $\Delta K_c=-1/+1$). It is further noted that in contrast to the sparse regions of S_1 chosen to illustrate differences in b-type and c-type features (see Figs. 3 and 4), it is nearly impossible to distinguish between them in these congested spectra.

With these general features in mind, numerous attempts have been made to fit these spectra using a Watson asymmetric rotor Hamiltonian. The GA parameters important for rapid convergence were first refined based on test runs of the S_1 origin regions. Furthermore, since b-type spectra are notoriously difficult to fit, additional software was written to enable much larger ranges in parameter space to be systematically sampled. This was accomplished by initiating massively parallel GA runs with each run focused in a narrow range of the total parameter space. The parameters of primary importance included ΔA, ΔB, and ΔC, two distortion constants Δ_J and Δ_K, two TDM orientation angles, and the rotational temperature. Large regions of parameter space were covered for geometries ranging from a T-shaped structure ($\Delta A \approx +100$ MHz) to a gable structure ($\Delta A = -200$ MHz). The lack of any apparent origin region required repeating each GA run at sequential 1 GHz intervals over the central 20 GHz regions of these spectra. Finally, the similar magnitudes of the B and C rotational constants required repeating these sequence runs to explore the possibility of axis interchange in the upper state. Unfortunately, all of these efforts failed to generate fits of the S_2 spectra, an issue to which we will return to below.

Despite the lack of rotational fits, the relative oscillator strengths of the S_1 and S_2 states in DPM provide important additional information regarding the excitonic interactions given in Eq. (3). Except for a small factor dependent on the ratio of transition energies, the relative oscillator strengths of the S_1 and S_2 states are directly proportional to the ratio of the integrated vibronic band intensities of these states. The S_1:S_2 ratio is reported in the supplemental material of Paper I (Ref. 14) as 5:1 or 83(3)%:17(3)% when reasonable estimates of the uncertainties are included. Combining this ratio

TABLE II. Experimental and calculated ground state rotational constants of DPM. The rotational parameters are also given for fitted structures where the two parameters α and τ defined in Fig. 1 were least-squares fitted to the observed moments of inertia.

	Expt.	B3LYP 6-31+G*			MP2 6-311++G**			MP2 cc-pVTZ		
		Opt.	Fit[a]	Opt.−Fit[b]	Opt.	Fit[a]	Opt.−Fit [b]	Opt.	Fit[a]	Opt.−Fit [b]
				DPM-h_{12} [c]						
A'' (MHz)	2036.5	2063.4	2029.2	+7.3	1981.1	2026.6	+9.9	1992.6	2035.4	+1.1
B'' (MHz)[d]	423.2	410.7	423.6	−0.4	435.9	423.8	−0.6	432.9	422.8	+0.4
C'' (MHz)	421.5	409.9	419.4	+2.1	429.6	418.6	+2.9	432.7	421.5	+0.0
α (deg)	⋯	114.8	111.7	**+3.1**	111.4	114.3	**−2.9**	111.9	114.6	**−2.7**
τ (deg)	⋯	56.7	55.0	**+1.7**	55.2	54.5	**+0.7**	58.3	57.8	**+0.5**
				DPM-d_{12} [e]						
A'' (MHz)	1682.1	1704.6	1681.3	+0.8	1641.3	1681.2	+0.9	1649.8	1682.1	+0.0
B'' (MHZ)[d]	382.3	371.6	383.3	−1.0	393.6	383.6	−1.3	391.4	383.0	−0.7
C'' (MHz)	381.7	370.3	378.3	+3.4	388.0	377.6	+4.1	390.5	381.6	+0.1
α (deg)	⋯	114.8	111.7	**+3.1**	111.4	114.3	**−2.9**	111.9	114.4	**−2.5**
τ (deg)	⋯	56.7	54.2	**+2.5**	55.2	53.8	**+1.4**	58.3	57.6	**+0.7**

[a]The fits were weighted according to the uncertainties propagated from the rotational constants.
[b]Observed minus fit values for rotational constants and optimized (Opt.) minus fit values for α and τ.
[c]Experimental rotational constants obtained from MW measurements and rounded for clarity.
[d]Axis designates the C_2 symmetry axis except for B3LYP optimized values where C_2 is along the c axis.
[e]Experimental rotational constants obtained from UV measurements and rounded for clarity.

with the S_1 TDM components given in Table I gives the relative oscillator strength components of 55(2)%:28(2)% along the $a:c$ axes for S_1 and 17(3)% along the b axis for S_2. A full discussion of the correspondence of these components with predictions from a dipole-dipole coupling model and *ab initio* theory is given below.

IV. DISCUSSION

The S_0 and S_1 rotational constants and the S_1 and S_2 TDM orientations determined here together with the relative band strengths of the S_1 and S_2 states from Paper I (Ref. 14) give us a framework to interpret the excitonic interactions in this flexible bichromophore. In this section, we will establish reasonable estimates of the S_0 and S_1 state geometries, address possible reasons why rotational fits of the S_2 origin bands so far have been elusive, and interpret the observed band strengths and exciton splitting in terms of a dipole-dipole coupling model parametrized in the flexible coordinates of DPM for comparison with predictions from quantum chemical theories.

A. S_0 and S_1 state geometries

The comparison of the observed ground state rotational constants with those predicted for the minimum energy structures at the B3LYP/6-31+G*, MP2/6-311++G**, and MP2/cc-pVTZ levels of theory[28] are given in Table II. While all predictions are within 3% of the observed values, systematic differences are seen at the two levels of theory. For example, the B'' and C'' rotational constants calculated by DFT are ≈3% smaller than the experimental values, while MP2 overestimates them by 2%–3%. Conversely, for A'', the DFT value is slightly larger by ≈1% while the MP2 value is ≈3% smaller than experiment. From normal mode analyses, both calculations predict a C_2 symmetric structure with the a inertial axis oriented perpendicular to the C_2 symmetry axis

and passing nearly through the centers of both rings. However, the inertial axis associated with the C_2 symmetry axis (either b or c) is different at the two levels of theory. The reason for this becomes clear from Fig. 7 where the rotational constants determined from the relaxed MP2 geometries are shown as a function of the torsional angle, τ ($\tau_1 = \tau_2$). This figure illustrates the sensitivity of the rotational constants to the torsional angle and the small change in τ (relative to the optimized value) required to switch these two axes.

In a similar way, minor changes along the "soft" coordinates τ and α (see Fig. 1) may easily account for the observed and calculated differences in the rotational constants. The optimized values of these variables from theory are reported in Table II together with values fitted to the experimental moments of inertia using the theoretical structures having all other structural parameters fixed. At each level of theory, the changes in α are similar for both isotopologues,
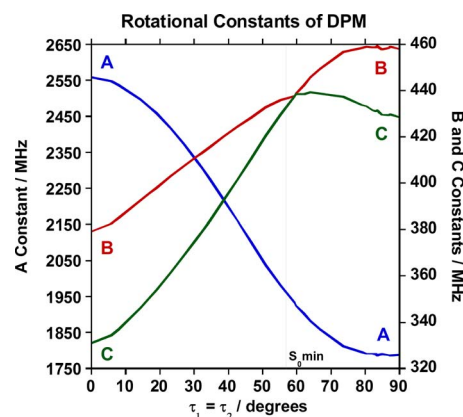

FIG. 7. (Color online) Theoretical rotational constants (MP2/6-311++G**) of DPM shown as a function of the ring torsional angle τ for the optimized C_2 symmetric structures. The equilibrium structure is designated with a vertical line and near the axis interchange angle of 59°.

increasing by $\approx 3°$ at the MP2 level but decreasing by $\approx 3°$ at the DFT level. The changes suggest either an underestimation of dispersive interactions at the DFT level or an overestimation at the MP2 level, the latter of which would tend to increase the attractive interactions between the rings and therefore decrease the bond angle α. In all cases, τ decreases by less than $3°$ to move the rings closer to a planar arrangement. Finally, we note the high quality of the structural predictions at the MP2/cc-pVTZ level where the fitted structures are nearly identical for both isotopologues with differences in the rotational constants of ≈ 1 MHz or less. From these results, it is clear that the rotational constants are sensitive functions of these variables and that τ and α of the ground state must be within a few degrees of $57°$ and $114°$, respectively.

From Table I, the changes in the rotational constants in S_1 are small. Similar least-squares fits of the S_1 observed moments to the configuration interaction singles (CIS)/6-311++G** excited state (C_2) geometry (*vide infra*) indicate slight decreases in the angles τ and α by $\approx 4°$ ($53.6°$ and $110.2°$ for DPM and $53.0°$ and $109.8°$ for DPM-d_{12}, respectively). This observation is consistent with the suggestion that diphenylamine tends toward planarity upon electronic excitation.[34] Also noteworthy is the magnitude of the change in τ, which is similar to the value of $|\Delta\tau| \approx 5.6°$ calculated from the harmonic torsional progression reported in Paper I.[14]

B. The S_2 states of DPM and DPM-d_{12}

The complexity of the rotational structure of the S_1 $+123$ cm^{-1} band of DPM and the S_1+116 cm^{-1} band of DPM-d_{12} is rather unusual for such low frequency vibronic bands built off the origin. For example, a study of the C_2 symmetric conformer of a similar molecule, bis-(2-hydroxyphenyl)methane,[35] has similar series of low frequency modes associated with the phenyl torsional motion. However, the rotationally resolved origin and four vibronic bands have been well fit to an asymmetric rotor Hamiltonian and all have a TDM orientation perpendicular to the C_2 axis consisting of 70%–75% a-type character. Moreover, from Paper I,[14] the state density of S_1 levels (of either symmetry) at these excess energies is less than 0.5 states/cm^{-1}, placing the S_2 origin in the sparse level coupled limit for vibronic coupling.[36]

To better understand why fits of the rotational structure of the S_2 states of DPM and DPM-d_{12} have so far been elusive, we have undertaken a study of the partially deuterated form, DPM-d_5, where one ring is fully deuterated. The full analysis of the rotationally resolved spectra of the S_1, S_1+T, $S_1+\bar{T}$, S_2, and $S_2+\bar{T}$ bands will be reported elsewhere.[37] For this discussion, the S_1 origin band (and S_1 vibronic bands) has been well fit to an asymmetric rotor Hamiltonian but now with a small TDM component along the b axis as expected from the reduction of symmetry. More importantly, the TDM orientation of the S_2 state acquires some $a:c$ hybrid-type character, giving this band a pronounced central Q branch and well-resolved P- and R-branch $K_a=1 \leftarrow 0$ series in J. These features remove any ambiguity regarding the

position of the S_2 origin and the changes in the upper state parameters in contrast to the b-type spectra of DPM and DPM-d_{12}. Despite these advantages, numerous attempts have still failed to fit the S_2 origin of DPM-d_5 to an asymmetric rotor model. Therefore, there remains little doubt that the rotational level structure of the S_2 states of DPM and DPM-d_{12} are also perturbed.

From the results of Paper I, four S_1 zero-order vibronic levels of A symmetry, $|S_1,050\rangle$, $|S_1,230\rangle$, $|S_1,410\rangle$, and $|S_1,031\rangle$ where $|v(T),v(\bar{T}),v(\beta)\rangle$, were found to mix with the S_2 origin of DPM (also of A symmetry) and have estimated coupling matrix elements ranging from 0.8 to 3.7 cm^{-1}. The A symmetry of these zero-order levels makes both Fermi and perpendicular Coriolis coupling mechanisms possible.[38] Given the number of states involved in DPM and DPM-d_{12}, analysis of such perturbations becomes intractable without first state-by-state assignments using double resonance methods. We also leave open the possibility that the eigenstates of S_2 arise from delocalized ("isomerization") states that sample other minima on the S_2 torsional surface.[39] Because of the relative simplicity of the S_2 spectrum of DPM-d_5, analysis that incorporates these perturbations is currently being explored.[37]

C. Dipole model predictions of the observed TDM orientation

Having good estimates of the S_0 and S_1 geometries of DPM, we now turn to predictions of the dipole-dipole coupling model given by Eq. (3). From the vibronic studies of Paper I and rotationally resolved data presented here, we have established that the S_1 and S_2 electronic excitations in DPM and DPM-d_{12} are delocalized across the toluene-like chromophores and the exciton states have relative oscillator strength components of 55(2)%:17(3)%:28(2)% along the $a:b:c$ principal axes. To understand these results within the dipole-dipole coupling model, the following equations were derived to predict the observed principal axis TDM components for any arbitrary orientation of the localized TDMs:

$$x = \cos\rho\,\sin\tau\,\cos\beta - \cos\tau\,\sin\beta, \tag{4a}$$

$$y = \left(\cos\tau\cos\frac{\alpha}{2}\cos\rho + \sin\rho\,\sin\frac{\alpha}{2}\right)\cos\beta$$

$$+ \sin\tau\cos\frac{\alpha}{2}\sin\beta, \tag{4b}$$

$$z = \left(\cos\tau\sin\frac{\alpha}{2}\cos\rho - \sin\rho\,\cos\frac{\alpha}{2}\right)\cos\beta$$

$$+ \sin\tau\sin\frac{\alpha}{2}\sin\beta, \tag{4c}$$

where x, y, and z (see Fig. 1) correspond to the c-, a- (S_1), and b-axis (S_2) principal axis projections of the delocalized TDMs, respectively. The relative intensities (and oscillator strengths) of each band type (specified as %$a:b:c$) are obtained directly by squaring these component amplitudes. In Eqs. (4a)–(4c), τ and α are the ring torsional and bending coordinates, respectively, defined in Figs. 1 and 2, and held

fixed to the fitted values of $\tau=57°$ and $\alpha=114°$ for the MP2/cc-pVTZ geometry (see Table II). The parameters ρ and β define the orientation of localized TDMs relative to the toluene subgroups as follows: ρ is the in-plane rotation angle where $\rho=0$ references an orientation perpendicular to the C–CH$_2$ axes and β is the out-of-ring-plane angle.

The simplest case that was considered by McClure[2] for crystalline DPM is that in which the localized TDMs are in plane and perpendicular to the C–CH$_2$ axes ($\rho=\beta=0°$) as it is in toluene. Equations (4) predict an $a:b:c$ component ratio of 9%:21%:70%, which is in poor agreement with the observed component ratio of the S_1 state. However, from previous gas-phase studies of substituted benzenes,[40] the in-plane rotation angles of the TDM were reported to be a sensitive function of not only the substituents but also their conformations. Varying the in-plane angle ρ to minimize differences between the observed and calculated intensity ratios gives a value of $\rho \approx 46°$ and a predicted ratio of 65%:1%:34%. While the S_1 ratio is now in good agreement, the S_2 relative intensity is much too small.

It is clear from the proceeding examples that in order to come into full agreement with observations, the out-of-plane terms in Eqs. (4) are needed. Such out-of-plane TDM character might be expected based on the close proximity of the two rings in DPM ($R_{\text{com}}=4$ Å) and the delocalized nature of all states involved in the transitions. Since only the orientation and not the direction of the TDMs is determined from the relative intensities, Eqs. (4a)–(4c) give the following four possible solutions for (ρ,β) that explain the observed intensity ratio (exactly): $(25°,20°)$, $(95°,66°)$, $(116°,20°)$, $(241°,14°)$ (for a given chiral isomer, equivalent pairs have $\rho \pm 180°$ for $-\beta$).

As a schematic illustration of one of these solutions, $(\rho,\beta)=(116°,20°)$, the orientations of the antisymmetric combination of the μ_{local} vectors are shown along three different view axes in Fig. 8. Also shown are the delocalized TDM vectors of the S_1 and S_2 states that result from the vector sums of the symmetric (not shown) and antisymmetric combinations of μ_{local}. The extent of the in-plane rotation and out-of-ring-plane character of μ_{local} becomes most evident in Fig. 8(c).

D. Dipole model predictions of the exciton splitting

The localized TDM orientations considered above are particularly relevant to the position and intensity of the upper exciton state since the in-plane and out-of-plane dependencies of the localized TDMs on τ will have a direct impact on the electronic coupling and hence splitting between the S_1 and S_2 states. After some vector algebra and substitutions in Eq. (3), the relative energy of the B state within the dipole approximation may be expressed in terms of the principal axis components as

$$V_{dd} = -\frac{\mu_A \mu_B}{4\pi\varepsilon_0 R^3}(2y^2 - (1-y^2)(1-2z^2))$$

$$= -\frac{\mu_A \mu_B}{4\pi\varepsilon_0 R^3}(3y^2 + 2z^2 - 2y^2z^2 - 1), \qquad (5)$$

where the leading negative sign gives the correct state order
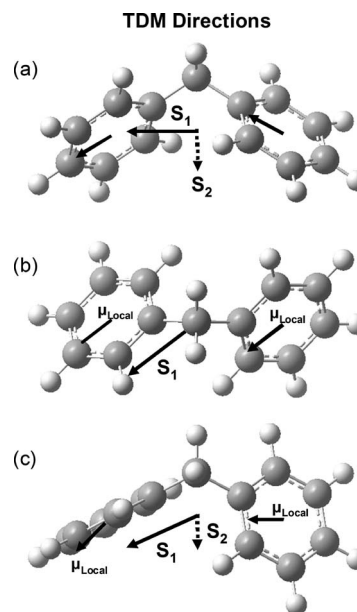

TDM Directions

(a)

(b)

(c)

FIG. 8. The delocalized TDM vectors of the S_1 and S_2 states of DPM that agree with observed relative intensity ratio. Also shown are the μ_{local} vectors of the S_1 state that were fitted to the dipole model for $(\rho,\beta)=(116°,20°)$. The corresponding directions of μ_{local} for the S_2 state (not shown) are the in-phase components. Projections are shown along the $x(c)$ axis in (a), along the $z(b)$ axis in (b), and along an axis 35° from z in the xz plane in (c) to illustrate the out-of-ring-plane component (left ring) and in-plane rotation (right ring) of μ_{local}. To reduce clutter and preserve phase, only one direction of all TDM vectors (which are double-headed arrows) is shown. The experimentally fitted MP2/cc-pVTZ geometry is shown in each panel ($\tau=57°$ and $\alpha=114°$).

in the limits of the planar ($\tau=0°$) and gable structures ($\tau=90°$). The relative energy of the A state is the negative of V_{dd}, and therefore V_{dd} is half the exciton splitting (this form is similar to that originally derived by McClure[2] except for the small contribution from the fourth-order term which was ignored there). The dependence of V_{dd} on τ, ρ, and β may be obtained following substitutions of Eqs. (4a)–(4c) into Eq. (5).

For the toluene-like case considered by McClure[2] (i.e., $\rho=\beta=0°$), a serious problem arises in the ordering of the exciton states of A and B symmetries. Predictions from this model are shown as dotted traces in Fig. 9(a) as a function of τ for $\alpha=114°$. Here, the inter-ring distance R used was 4 Å and the localized TDMs were estimated as intermediate between the calculated S_1 and S_2 TDMs in toluene (1.5×10^{-30} C m or 0.45 D). Figure 9(a) clearly shows that the lower energy state has A symmetry near the observed S_0 geometry, in clear disagreement with our results. Indeed, McClure[2] assigned the lower exciton state observed in the crystal to the A state based on this order. However, when in-plane and out-of-plane rotations of the localized TDMs are taken into account, the state order reverses for all (ρ,β) pairs determined from the observed band intensities, $(25°,20°)$, $(95°,66°)$, $(116°,20°)$, $(241°,14°)$. The values of these angles suggest that near the S_0 geometry, through space interactions from molecular orbital overlap on the two rings not only leads to significant out-of-plane TDM character but also causes the localized TDMs to rotate away from that of toluene ($\rho=0°$).[40] As a result, the increasing head-to-
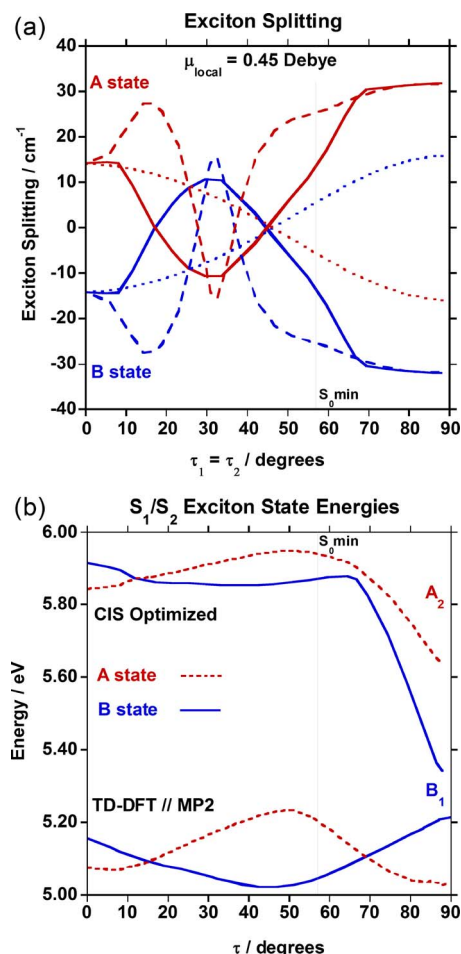
FIG. 9. (Color online) Energies of the exciton levels for C_2 symmetric structures from (a) the dipole-dipole coupling model and (b) TD-B3LYP//MP2 and CIS levels of theory (6-311++G** basis sets) as a function of the ring torsion angle τ. The splitting are shown in (a) for $\rho = \beta = 0°$ (dotted lines), ρ and β from CIS (solid lines), and ρ and β from TD-DFT (dashed lines).

tail alignment with increasing τ for the antisymmetric TDM combination is the principal reason why the *B* state moves to lower energy in Fig. 9(a). Furthermore, since all terms in Eq. (5) are independent of possible sign differences for the *y* and *z* components, all (ρ, β) pairs give exactly the same exciton

splitting of 26 cm^{-1}. This is more than four-fold smaller than the observed value of +123 cm^{-1}. In Sec. IV E, we seek a further understanding of these results with the aid of *ab initio* theory.

E. TDM orientations and exciton splittings from *ab initio* theory

In this section, we examine the quality of *ab initio* predictions of the S_1/S_2 TDM orientations, exciton state order, and energy splitting and interpret these results in terms of the dipole model parameters. Table III summarizes some of the key findings from the excited state calculations at the TD-B3LYP,[28] CIS,[28] and CASSCF (Ref. 29) levels of theory. For TD-DFT, single point energy calculations were performed on the MP2/6-311++G** optimized ground state geometries because system size prohibits numerical geometry optimizations in G03.[28] Furthermore, fully relaxed excited state geometry optimizations performed using CIS with various basis sets break the C_2 symmetry of DPM.[14] Since this symmetry reduction is in direct contradiction with our observations, the results in Table III and elsewhere are restricted to geometries with C_2 symmetry.

From comparisons with the results in Table III, predictions from TD-DFT overestimate the *a*-type intensity of S_1 by 30% and underestimate the S_2 band strength by 9%; CIS *underestimates* the former by $\approx$20% and *overestimates* the latter by 9%. While both calculations correctly predict the exciton state order for τ near the S_0 geometry, they vastly overestimate the exciton splitting by more than five-fold in contrast to the value of 135 cm^{-1} predicted by CASSCF(8,8).

While such discrepancies appear to present serious limitations of the former two theories, the strong dependence of the TDM orientation on τ from Eqs. (4) and exciton splitting from Eq. (5) warrants a closer look. The S_1 and S_2 state energies shown in Fig. 9(b) for $\tau \equiv \tau_1 = \tau_2$ illustrate this point. As expected for excitonic interactions between two states, the minima on S_1 have corresponding maxima on S_2. State reversals at the TD-DFT level occur at $\tau \approx 15°$ and 69° with S_2 minima appearing near the planar and gable geometries. The +123 cm^{-1} splitting observed occurs at $\tau \approx 66°$ or just

TABLE III. Results of excited state calculations on DPM.

	Expt.	CIS^a 6-311++G**	TD-B3LYP^b 6-311++G**	CASSCF(8,8)^b 6-31G*
$S_1(B)$ (eV)	4.64	5.86	5.04	6.87
$S_2(A)$ (eV)	4.66	5.95	5.22	6.88
$\Delta_{12}{}^e$ (cm^{-1})^c	+123	+697	+1429	+136
				$\cdots$
$a:b:c$ (%)	55(2):17(3):28(2)^d	35:26:39	85:8:7	e
α (deg)	114^f	113.9	111.4^g	112.0^g
τ (deg)	57^f	50.3	55.2^g	58.4 ^{g}

^{a}Constrained to C_2 symmetry. Fully optimized geometry has C_1 symmetry.
^{b}Vertical excitation energies.
^{c}Exciton splitting between S_1 and S_2 states.
^{d}Ratio determined from TDM of S_1 and integrated intensities of vibronic bands from Ref. 14.
^{e}TDMs were not obtained from the CASSCF calculations.
^{f}S_0 estimates based on fits to MP2/cc-pVTZ geometry given in Table II.
^{g}Geometries fixed at optimized MP2 ground state geometry at the same level of theory.

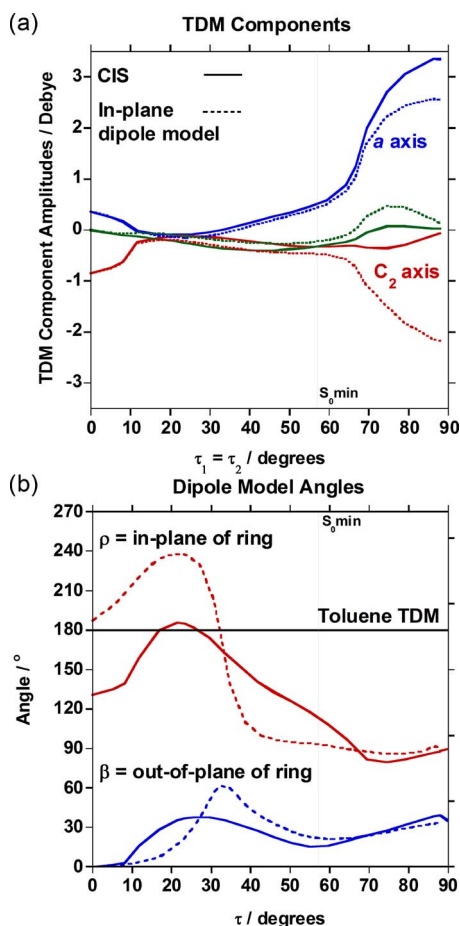(a) **TDM Components**

(b) **Dipole Model Angles**

FIG. 10. (Color online) (a) The TDM components (in Debye) of DPM predicted by CIS/6-311++G** (solid lines) and the in-plane dipole model (dashed lines). (b) In-plane angles ρ and out-of-plane angles β of the dipole model that describe the TDM components from CIS (solid lines) and TD-DFT (dashed lines) in (a). The optimized values of the inter-ring angle α are included in the dipole model as a function of the ring torsion angle τ and range between 100° and 130° for both calculations.

(a) **Relative Band Strengths**

(b) **Relative Band Strengths**

FIG. 11. (Color online) The relative band strengths as a function of the ring torsion angle τ in the principal axis frame of DPM at the (a) CIS and (b) TD-B3LYP//MP2 levels of theory (6-311++G** basis sets). The best correspondence with the observed components occurs near $\tau \approx 57°$ from CIS and $\approx 54°$ from TD-DFT.

$\approx 8°$ greater than the S_0 minimum. For the relaxed CIS geometries, a similar state reversal occurs near the planar geometry ($\tau \approx 12°$) and the states approach the observed splitting near 69° but avoid crossing there. Interestingly, both states from CIS have deep minima predicted for the gable structure far below the vertical excitation region from S_0. We also voice caution that while the S_2 states at both levels would appear not to support wave function amplitude near the excitation region, the full 2D excited state surfaces (similar to that of Fig. 2) are needed for any conclusive assessment.

At the CIS level, the τ dependence of the TDM principal axis components (in Debye) for the S_1 and S_2 states are shown as solid lines in Fig. 10(a). The components predicted by the dipole model using Eqs. (4a)–(4c) are also shown as dotted lines in Fig. 10(a) for values of ρ that give the best (rms) agreement with CIS. The corresponding best fit values of ρ are shown as the top trace (solid line) in Fig. 10(b) together with the results from a similar calculation using TD-DFT (dashed lines). As expected, deviations from the in-plane dipole predictions are least important when the two rings are nearly coplanar (i.e., $\tau \approx 0$). However, for $\tau > 20°$,
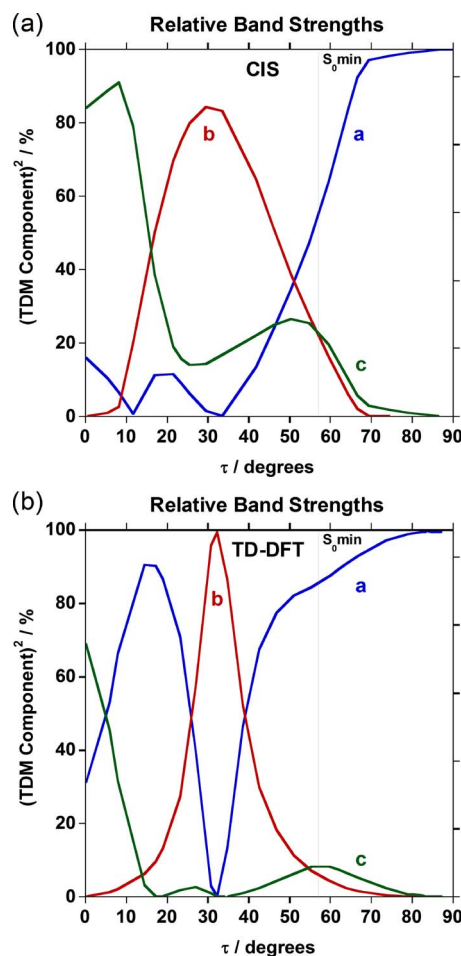
significant deviations occur at both levels of theory that require use of the out-of-plane β terms in Eqs. (4a)–(4c). The values of β and ρ required to completely describe the CIS and TD-DFT TDM components are also shown in Fig. 10(b). Here, ρ remains essentially unchanged from the in-plane case where it approaches 90° for $\tau > 60°$. For $\tau > 20°$, β values as large as 60° suggest that inter-ring orbital penetration effects make significant contributions to the TDM as the π and π^* orbitals on the two rings begin to overlap.

The CIS predictions of the relative band strengths, $\%a:b:c$, are shown as a function of τ in Fig. 11(a) (solid lines). The best agreement with the observed ratio of 55(2)%:17(3)%:28(2)% occurs near the ground state τ value of 57° and $(\rho, \beta) = (114°, 15°)$ with intensity components of 55%:23%:22%. The TD-DFT results shown in Fig. 11(b) are not as satisfactory. The best match occurs for $\tau \approx 54°$ and $(\rho, \beta) = (93°, 23°)$ with band strengths of 84%:8%:8%. At either level, the reasonable correlation of intensities is sufficient to identify only one of the four possible experimentally fit (ρ, β) pairs as $(116°, 20°)$ or equivalently $(-64°, -20°)$. The observed TDM vector representations for this solution were shown earlier in Fig. 8.

The dipole model exciton splittings that correlate to the

ab initio TDM components are shown in Fig. 9(a) for a fixed value of $\mu_{local}=0.45$ D. At the best fit τ values, the CIS/dipole splitting (solid lines) is less than one-fourth the observed value and less than one-half observed at the TD-DFT/dipole level (dashed lines). Again, while these discrepancies seem large, the magnitudes of the TDMs from CIS in Fig. 10(a) rapidly increase for increasing τ and if used in place of μ_{local} in Eq. (5) would reproduce the observed splitting at $\tau \approx 67°$.

The better overall agreement of the relative band strengths at the CIS level suggests that optimization of excited state geometries may be an important factor to arrive at an accurate description of the excitonic interactions in DPM. Furthermore, the out-of-ring-plane component of μ_{local} appears to play a significant role in all excitonic descriptions of DPM, suggesting that in-plane models may be insufficient to capture the essential photophysics of non-coplanar exciton coupled chromophores in close proximity.

We note in closing that out-of-plane TDM character in gas-phase benzene (and other aromatic) chromophores is rather unusual. For example, East *et al.*[7] investigated excimer formation in a similar but more extended system, 1,3-diphenylpropane, using rotationally resolved methods and made definitive assignments of four torsional isomers based on rotational contour analyses. The TDM orientations observed for two of the bands were attributed to the vector sums of the localized TDMs of the benzene subgroups while the other two bands were assigned to uncoupled excitations on separate rings of one conformer. In each case, the analysis and assignment were based only on the in-plane TDMs of the rings. However, out-of-ring-plane character may be of more importance in strongly coupled exciton systems that contain significant components from charge transfer states. For example, such character may be necessary to explain the optical polarization properties of the delocalized states of molecular crystals[41] and the electron transport propensities in dendrimers where variable exciton coupling was linked to enhanced contributions from charge transfer states upon excited state relaxation.[8]

V. CONCLUSIONS

Analyses of rotationally resolved data of the ground and exciton coupled S_1/S_2 origin regions of DPM and DPM-d_{12} have clarified the global spatial extent of the molecular orbitals involved, the symmetry assignments of these states, and, in former cases, the molecular geometries. The $S_1 \leftarrow S_0$ spectra of both isotopologues are $a:c$ hybrid bands and are well fit to asymmetric rotor models in both states, establishing the lower energy S_1 states as delocalized antisymmetric combinations of the locally excited states of the toluene-like subgroups. In contrast, the $S_2 \leftarrow S_0$ spectra of DPM and DPM-d_{12} which appear at low excess energies in S_1 (+123 and +116 cm^{-1}, respectively), display b-type spectra, are perturbed, and consequently have not been assigned. The perturbed rotational structure of the S_2 states is likely a result of Coriolis- or Fermi-type mixing with the four nearby S_1 vibronic bands that were identified in the previous R2PI and SVLF studies[14] to have T, $\bar{T}$, and β vibrational state charac-

ter. Possible contributions from isomerization states[39] arising from other minima on the 2D torsional surface may also contribute to the complexity of these spectra.

The relative intensities of the TDM components, the S_1/S_2 exciton splitting, and the geometries obtained from these two studies are used to assess the predictive quality of the classical dipole coupling model and excited state results at modest levels of quantum theory. We find that the in-plane dipole coupling model is insufficient and that out-of-ring-plane dipole coupling terms are needed to fully account for the observed TDM orientations. We also show that CIS predictions on optimized excited state structures appear to provide a more comprehensive picture of the excitonic interactions in DPM. We further acknowledge the need to explore the impact of high order multiple terms (dipole-quadrupole, dipole-octupole, etc.)[5] in the classical expansion of the Coulomb potential and application of multiconfiguration, multireference [multiconfiguration-reference configuration interaction (MRCI),[42] multiconfiguration self-consistent field (MCSCF)[43]], or novel single reference coupled-cluster [equation of motion coupled-cluster (EOM-CC),[44] coupled-cluster singles and doubles (CC2)[45]] *ab initio* quantum methods to arrive at a more complete understanding of the excitonic interactions in this bichromophore.

ACKNOWLEDGMENTS

[1] R. Coffman and D. S. McClure, Can. J. Chem. **36**, 48 (1958).
[2] D. S. McClure, Can. J. Chem. **36**, 59 (1958).
[3] E. Arunan and H. S. Gutowsky, J. Chem. Phys. **98**, 4294 (1993).
[4] N. A. van Dantzig, D. H. Levy, C. Vigo, and P. Piotrowiak, J. Chem. Phys. **103**, 4894 (1995).
[5] G. D. Scholes and K. P. Ghiggino, J. Phys. Chem. **98**, 4580 (1994).
[6] S. C. Abrahams, J. M. Robertson, and J. G. White, Acta Crystallogr. **2**, 238 (1949); D. W. Cruickshank, *ibid.* **10**, 504 (1957).
[7] A. L. L. East, P. Cid-Aguero, H. Liu, R. H. Judge, and E. C. Lim, J. Phys. Chem. A **104**, 1456 (2000).
[8] A. L. Thompson, K. M. Gaab, J. Xu, C. J. Bardeen, and T. J. Martinez, J. Phys. Chem. A **108**, 671 (2004).
[9] T. Fujiwara, M. Z. Zgierski, and E. C. Lim, J. Phys. Chem. A **112**, 4736

(2008).

[10] E. A. Lipman, B. Schuler, O. Bakajin, and W. A. Eaton, Science **301**, 1233 (2003).

[11] Z. J. Donhauser, B. A. Mantooth, K. F. Kelly, L. A. Bumm, J. D. Monell, J. J. Stapleton, D. W. Price, Jr., A. M. Rawlett, D. L. Allara, J. M. Tour, and P. S. Weiss, Science **292**, 2303 (2001).

[12] J. J. Hopfield, Phys. Rev. **112**, 1555 (1958).

[13] M. Feigel, J. Mol. Struct. **366**, 83 (1996).

[14] N. R. Pillsbury, J. A. Stearns, C. W. Müller, T. S. Zwier, and D. F. Plusquellic, J. Chem. Phys. **129**, 114301 (2008).

[15] D. P. Craig and P. C. Hobbins, J. Chem. Soc. **1955**, 539.

[16] M. A. El-Sayed and G. W. Robinson, Mol. Phys. **4**, 273 (1961).

[17] M. Kasha, H. R. Rawls, and M. El-Bayoumi, Pure Appl. Chem. **11**, 371 (1965).

[18] N. A. van Dantzig, D. H. Levy, C. Vigo, and P. Piotrowiak, J. Chem. Phys. **103**, 4894 (1995).

[19] T. M. Halasinski, J. L. Weisman, R. Ruiterkamp, T. J. Lee, F. Salama, and M. Head-Gordon, J. Phys. Chem. A **107**, 3660 (2003).

[20] A. Held and D. W. Pratt, J. Chem. Phys. **96**, 4869 (1992).

[21] A. Müller, F. Talbot, and S. Leutwyler, J. Chem. Phys. **116**, 2836 (2002).

[22] D. F. Plusquellic, S. R. Davis, and F. Jahanmir, J. Chem. Phys. **115**, 225 (2001).

[23] L. E. Jusinski and C. Taajes, Rev. Sci. Instrum. **72**, 2837 (2001).

[24] W. A. Majewski and W. L. Meerts, J. Mol. Spectrosc. **104**, 271 (1984).

[25] D. F. Plusquellic, R. J. Lavrich, T. Petralli-Mallow, S. R. Davis, T. M. Korter, and R. D. Suenram, Chem. Phys. **283**, 355 (2002).

[26] E. Riedle, S. H. Ashworth, J. T. Farrell, Jr., and D. J. Nesbitt, Rev. Sci. Instrum. **65**, 42 (1994); D. F. Plusquellic, O. Votava, and D. J. Nesbitt, Appl. Opt. **35**, 1464 (1996).

[27] R. D. Suenram, J. U. Grabow, A. Zuban, and I. Leonov, Rev. Sci. Instrum. **70**, 2127 (1999); A. R. H. Walker, W. Chen, S. E. Novick, B. D. Bean, and M. D. Marshall, J. Chem. Phys. **102**, 7298 (1995).

[28] M. J. Frisch, G. W. Trucks, H. B. Schlegel et al., GAUSSIAN03, Revision C.01 Gaussian Inc., Pittsburgh, PA, 2004.

[29] M. W. Schmidt, K. K. Baldridge, J. A. Boatz, S. T. Elbert, M. S. Gordon, J. H. Jensen, S. Koseki, N. Matsunaga, K. A. Nguyen, S. J. Su, T. L. Windus, M. Dupuis, and J. A. Montgomery, J. Comput. Chem. **14**, 1347 (1993).

[30] J. A. Hageman, R. Wehrens, R. de Gelder, W. L. Meerts, and L. M. C. Buydens, J. Chem. Phys. **113**, 7955 (2000); M. Schmit and W. L. Meerts, in Handbook of High Resolution Spectroscopy, edited by M. Quack and F. Merkt (Wiley, New York, 2008).

[31] W. A. Majewski, J. F. Pfanstiel, D. F. Plusquellic, and D. W. Pratt, in Laser Techniques in Chemistry, edited by A. B. Myers and T. R. Rizzo (Wiley, New York, 1995), Vol. XXIII; D. F. Plusquellic, R. D. Suenram, B. Maté, J. O. Jensen, and A. C. Samuels, J. Chem. Phys. **115**, 3057 (2001).

[32] Y. R. Wu and D. H. Levy, J. Chem. Phys. **91**, 5278 (1989); G. Berden, W. L. Meerts, and E. Jalviste, ibid. **103**, 9596 (1995).

[33] F. J. Lovas (unpublished).

[34] I. V. Tretiakov and J. R. Cable, J. Chem. Phys. **107**, 9715 (1997).

[35] N. R. Pillsbury, C. W. Müller, T. S. Zwier, and D. F. Plusquellic, "Conformational effects on excitonic interactions in a prototypical H-bonded bichromophore: Bis(2–hydroxyphenyl)methane," J. Phys. Chem. A. (submitted).

[36] J. Jortner, Faraday Discuss. **108**, 1 (1997).

[37] N. R. Pillsbury, C. W. Müller, T. S. Zwier, D. F. Plusquellic and J. R. Cable (unpublished).

[38] R. W. McKellar, D. W. Tokaryk, and D. R. T. Appadoo, J. Mol. Spectrosc. **244**, 146 (2007); A. R. W. McKellar and D. R. T. Appadoo, ibid. **250**, 106 (2008).

[39] E. Hudspeth, D. A. McWhorter, and B. H. Pate, J. Chem. Phys. **107**, 8189 (1997); D. A. McWhorter and B. H. Pate, J. Phys. Chem. A **102**, 8795 (1998).

[40] R. T. Kroemer, K. R. Liedl, J. A. Dickinson, E. G. Robertson, J. P. Simons, D. R. Borst, and D. W. Pratt, J. Am. Chem. Soc. **120**, 12573 (1998).

[41] D. P. Craig and S. H. Walmsley, Excitons in Molecular Crystals (Benjamin, New York, 1968); S. B. Singham and D. W. Pratt, J. Phys. Chem. **86**, 507 (1982).

[42] H.-J. Werner and P. J. Knowles, J. Chem. Phys. **89**, 5803 (1988).

[43] G. M. Chaban, J. Lundell, and R. B. Gerber, J. Chem. Phys. **115**, 7341 (2001).

[44] J. Geertsen, M. Rittby, and R. J. Bartlett, Chem. Phys. Lett. **164**, 57 (1989); J. F. Stanton and R. J. Bartlett, J. Chem. Phys. **98**, 7029 (1993); K. Kowalski and P. Piecuch, ibid. **115**, 643 (2001).

[45] O. Christiansen, H. Koch, and P. Jørgensen, Chem. Phys. Lett. **243**, 409 (1995).